Journal of Hydrology (2008) 353, 129–142

available at www.sciencedirect.com

ScienceDirect

journal homepage: www.elsevier.com/locate/jhydrol

Fully conservative coupling of HEC-RAS with MODFLOW to simulate stream–aquifer interactions in a drainage basin

Leticia B. Rodriguez [a,*], Pablo A. Cello [b,1], Carlos A. Vionnet [a,2], David Goodrich [c]

[a] Department of Hydrology and Water Resources, University of Arizona, Tucson, AZ USA
[b] Facultad de Ingenierìa y Ciencias Hìdricas, Universidad Nacional del Litoral, CC 217, 3000 Santa Fe, Argentina
[c] Southwest Watershed Research, Agricultural Research Service, U.S. Department of Agriculture, 2000 East Allen Road, Tucson, AZ 85719, USA

Received 20 September 2007; received in revised form 10 January 2008; accepted 6 February 2008

KEYWORDS
Groundwater–surface water interaction;
Hydrologic modelling;
MODFLOW;
HEC-RAS

Summary This work describes the application of a methodology designed to improve the representation of water surface profiles along open drain channels within the framework of regional groundwater modelling. The proposed methodology employs an iterative procedure that combines two public domain computational codes, MODFLOW and HEC-RAS. In spite of its known versatility, MODFLOW contains several limitations to reproduce elevation profiles of the free surface along open drain channels. The Drain Module available within MODFLOW simulates groundwater flow to open drain channels as a linear function of the difference between the hydraulic head in the aquifer and the hydraulic head in the drain, where it considers a static representation of water surface profiles along drains. The proposed methodology developed herein uses HEC-RAS, a one-dimensional (1D) computer code for open surface water calculations, to iteratively estimate hydraulic profiles along drain channels in order to improve the aquifer/drain interaction process. The approach is first validated with a simple closed analytical solution where it is shown that a Piccard iteration is enough to produce a numerically convergent and mass preserving solution. The methodology is then applied to the groundwater/surface water system of the Choele Choel Island, in the Patagonian region of Argentina. Smooth and realistic

* Corresponding author. Permanent address: Facultad de Ingenierìa y Ciencias Hìdricas, Universidad Nacional del Litoral, CC 217, 3000 Santa Fe, Argentina. Tel.: +1 54 342 4575234x198; fax: +1 54 342 4575224.
E-mail address: leticia@fich1.unl.edu.ar (L.B. Rodriguez).
[1] Present address: Department of Civil Engineering, University of Illinois, Urbana-Champaign, IL, USA.
[2] Present address: Facultad de Ingenierìa y Ciencias Hìdricas, Universidad Nacional del Litoral, CC 217, 3000 Santa Fe, Argentina.

0022-1694/$ - see front matter
doi:10.1016/j.jhydrol.2008.02.002

hydraulic profiles along drains are obtained while backwater effects are clearly represented.

Introduction

To determine the amount of water that is being exchanged at any time at any given location between open channel and its surrounding aquifer poses a problem that not only has attracted the interest of the scientific community but also has many environmental implications. On one hand, depletion of streamflows and wetlands due to groundwater withdrawals often affects transient surface water flows, which in turn, are critical to sustain protected flora and wildlife. On the other hand, poorly drained soils due to a malfunctioning drainage system may result in a build up of the water table that can impact the productivity of irrigated land (Skaggs et al., 1995; Johnson and Koenig, 2003). Groundwater discharge to the drain ceases when the water head in the aquifer drops at/or below the elevation of the channel drain bottom. In actuality, groundwater discharge to channel drains can be regarded as a one-way stream–aquifer interaction problem. Therefore, the aquifer-to-drain flux and stream–aquifer interactions can be studied with a similar methodology, as long as the exchange flux can be characterized with a Newton's type cooling law (Carslaw and Jaeger, 1959), driven by the hydraulic head difference between the two systems. Part of the objective of the present work is to show that the vast experience gained over the years on the treatment of stream–aquifer interactions (Sophocleous, 2002) carries over intact to the analysis of the drainage flow-groundwater discharge problem mentioned above. Specifically, this work was motivated by a particular situation (Rodríguez et al., 2006) encountered when high elevation free surface flows that surround a shallow aquifer overlap with the irrigation season. In this situation, the high river flows interfere with groundwater discharge through the drainage system.

Drainage of water from the soil profile is essential for the proper functioning of intensely irrigated agricultural areas in semiarid regions to remove excess water and evapoconcentrated salts from the root zone. Natural drainage from irrigated areas accounts for a portion of unsaturated and saturated flow to streams and vertical seepage to underlying aquifers. Artificial drainage water is usually discharged by a network of canals and ditches, a fraction of which stays in the system and eventually builds up the water table. The drainage efficiency depends, among other factors, on the interaction with the groundwater flow, the hydraulic conditions at the drain discharging points, and the maintenance of the drainage network (ILRI, 1994). Modelling provides a rapid analysis tool for obtaining a better understanding of the behaviour of these complex systems. For example, the representation of a drainage network in MODFLOW is accomplished through the DRAIN Module (DRN) (McDonald and Harbaugh, 1988). MODFLOW is a computational code that numerically solves the 3D form of the groundwater flow governing equation. The groundwater flow toward drains, known as drain flow, is assumed to be proportional to the difference between the hydraulic head within the drain and the hydraulic head in the adjacent aquifer. The MODFLOW DRN is a one-way flux package, whereby only aquifer-to-drain flows are allowed, and not the reverse. Input parameters to the module include the water elevation in the drain, or drain head, the spatial location of the drain, and the drain conductance. The drain head must be externally calculated by the modeller based on field data. When field data are limited, interpolation and/or extrapolation is needed to compute drain heads for each hydrologic condition spanned by the simulation. This task may be quite cumbersome and entails many uncertainties when dealing with intricate drainage networks. In addition to the difficulty and uncertainty of extensive space and time interpolation, neither surface flow backwater effects nor surface flow propagation is handled by the module. In actuality, as stated by McDonald and Harbaugh (1988), *''with proper selection of coefficients, the RIVER Module could be used to perform the functions of the DRAIN Module''*. However, this alternative would still maintain the limitations previously itemized.

Pohll and Guitjens (1994) employed MODFLOW to simulate regional flow and flow to the drains. Batelaan and De Smedt (2004) also used MODFLOW with its DRN Module to analyze the protection and development of groundwater-dependent wetlands. Their work pointed out conceptual and practical problems in the calculation of groundwater discharge by the DRN Module (e.g., calculating water tables above the land surface, difficult conductance parameterization, and large water balance errors). To overcome these problems, a new SEEPAGE package for MODFLOW was developed, which resulted in more accurate results in comparison with those obtained with the DRN Module. The DRT1 Package (Banta, 2000) allows to specify a certain fraction of the simulated drain flow to be returned to any cell in the system, as opposed to the DRN Module in which drain flow was removed from the system. However, channel drain flow calculations follow those implemented on the DRN Package.

Thus, in spite of the considerable progress made in recent years, a freely available model that couples groundwater discharge to a drainage network flow, where backwater effects on the free surface along the channel drains are taken into account is not available. In this study, the open source, highly tested and widely known HEC-RAS computer program is linked to MODFLOW in an iterative way in order to improve the drain flow–aquifer discharge problem. The main objective of the approach is to obtain a more physically realistic hydraulic profile in channel drains within a regional groundwater flow system. With the aid of a simple analytical solution, it is then established that the proposed scheme is numerically convergent and mass conserving. Therefore, the paper is organized as follows: a brief review of numerous relevant works accumulated on the subject of stream–aquifer interaction is presented first. A simple approximate analytical solution for the coupling problem,

which provides the mathematical setting for the proposed approach is discussed in the section ''Simplified analytical solution'', following the mathematical model posed in the section ''A fully coupled mathematical model''. Numerical results to the analytical solution obtained with a Piccard iteration between HEC-RAS and MODFLOW are covered in the section ''Numerical solution with HEC-RAS/MODFLOW''. In the section ''Application to the Choele Choel Island, Patagonia, Argentina'', the approach is used to analyze the water table build up problem in the shallow aquifer of the Choele Choel Island, in the Patagonian region of Argentina, where the case was first studied with the DRN Module, and now is addressed with HEC-RAS instead. Conclusions are drawn in the section ''Conclusion''.

Surface water–groundwater interactions

It is worth noting that the current study is limited to the case of groundwater discharge to the surface water and not the reverse. Nonetheless, the subject of stream/aquifer interactions is reviewed from a broad perspective as the approach here introduced is general enough to handle both cases.

Over the years, numerous approaches have been developed to tackle stream–aquifer interaction problems. An overview of the state-of-the-art can be found in the recent work of Sophocleous (2002). Analytical studies of the linearized 1D Boussinesq equation to describe changes in bank storage caused by temporal variations in water elevation of the adjacent channel have been pursued by Cooper and Rorabaugh (1963), Hogarth et al. (1997), Moench and Barlow (2000), and Hantush, 2005), whereas its nonlinear counterpart problem has been analyzed by Serrano and Workman (1998) and Parlange et al. (2000), among others. The analytical work of Theis (1947) on streamflow depletion by pumping was revisited and expanded by Hunt (1999), among many contributors to the subject. Recently, stream–aquifer exchange was also assessed using inverse modelling (Szilagyi et al., 2005), and parameter uncertainty was addressed with stochastic modelling by Srivastava et al. (2006). In a multidimensional setting, the numerical solution of a fully conservative, integrated groundwater/surface water modelling was pioneered by Pinder and Sauer (1971), whose simplified solution was presented years later by Hunt (1990) with the linearized form of the kinematic wave approximation. Numerous modelling studies concentrated on capturing the regional water balance, a trend mainly favoured by the widespread use of the code MODFLOW in combination with the Streamflow Routing (STR1) Package (Prudic, 1989). The STR1 Package solves a water budget along each stream reach, where the surface water discharge is computed with the aid of Manning's boundary resistance relationship based on a prevailing normal streamflow assumption that is seldom attained in practice. However, its simplicity and mass preserving properties made it the commonly chosen tool to simulate stream–aquifer interactions. Further attempts to improve the approximation were made with MODBRANCH (Swain and Wexler, 1996), which essentially recovered the mathematical model of Pinder and Sauer (1971), and with the two well-documented USGS releases DAFLOW (Jobson and Harbaugh, 1999) and SFR1 (Prudic et al., 2004). DAFLOW computes unsteady streamflows by means of diffusive wave routing, where the stream–aquifer exchange is simulated as a streambed leakage. The SFR1 Package replaces the former Prudic's STR1 package (Prudic, 1989) to simulate stream–aquifer interaction with MODFLOW-2000 (Harbaugh et al., 2000). Other improvements directed at increasing MODFLOW capabilities to deal with the coupled surface–subsurface water systems are presented in Panday and Huyakorn (2004), whose code MODHMS is also based upon the diffusive wave approximation of the 1D Saint Venant equations. MODHMS was recently applied by Werner et al. (2006) to study the stream–aquifer interactions in a tropical catchment in north-eastern Australia. Sophocleous et al. (1999) linked the surface water code SWATMOD with MODFLOW to study the stream–aquifer interactions on a basin in south-central Kansas, USA. A similar approach was later followed by Sophocleous and Perkins (2000) to link SWAT to MODFLOW. The approach taken herein is in tune with the emphasis given by Sophocleous and Perkins (2000) on the practicality and advantages of using conceptually simple approaches to address integrated dynamic modelling.

A fully coupled mathematical model

Assuming invariant properties such as hydraulic conductivity in the saturated porous medium and boundary resistance in the channel bed, the coupling between the conservation law of a groundwater flow and the conservation of mass and momentum fluxes of an open channel flow, can be posed mathematically as follows:

$$S_y \frac{\partial \Phi}{\partial T} - \nabla \cdot T_r \nabla \Phi = R \quad \text{on } \Omega, \tag{1}$$

$$\frac{\partial A}{\partial T} + \frac{\partial Q}{\partial S} = D \quad \text{on } \Gamma, \tag{2}$$

$$\frac{\partial Q}{\partial T} + \frac{\partial}{\partial S}\left(\frac{Q^2}{A}\right) + gA\frac{\partial H}{\partial S} = gA(S_o - S_F) \quad \text{on } \Gamma. \tag{3}$$

Eq. (1) governs the depth averaged flow in the porous medium within the Dupuit–Forchheimer approximation (Bear, 1972), while Eqs. (2) and (3) are known as the Saint Venant's equations (Chow et al., 1988), or the long wave approximation which is valid whenever the pressure in the water column is distributed hydrostatically. For the problem considered here, the lateral interacting flux D per unit length of channel [L^2T^{-1}] in Eq. (2) is given by

$$D = \Lambda[\Phi - (H + Z_b)] \quad \text{on } \Gamma. \tag{4}$$

As it will be shown shortly, D can be related to R through a very simple mathematical expression. With reference to Fig. 1, the variables used above are defined as follows: S_y is the aquifer storativity coefficient, Φ is the aquifer head [L] above datum as function of the horizontal coordinates $\boldsymbol{X} = (X, Y)$ and time T, ∇ is the 2D horizontal gradient operator [L^{-1}], T_r is the aquifer transmissivity [L^2T^{-1}], which depends upon the aquifer head, R is the net recharge [LT^{-1}] from rainfall and/or irrigation applied over the area Ω [L^2], Λ is the reciprocal of the hydraulic impedance of the

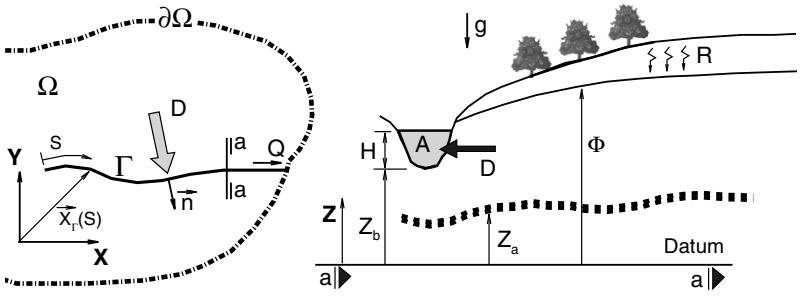

Figure 1 Sketch of the conceptual model. (left) Plan view of a regional phreatic aquifer of planar area Ω discharging onto an open drain channel. ∂Ω represents a portion of Ω's external boundary. (right) Cross-section a—a.

streambed material [LT^{-1}], H is the water depth [L] in the stream Γ, whose location in the horizontal plane is parameterized with $\boldsymbol{X} = \boldsymbol{X}_\Gamma(S)$, where S is the arc length [L] in the streamwise direction, A is the wetted area [L^2] of the flowing stream cross-section, Q is the volumetric stream discharge [L^3T^{-1}], S_o is the channel bed slope, $=-dZ_b/dS$ for a fixed bed, where Z_b is the streambed elevation [L] above datum measured along the vertical coordinate Z, which is aligned with the acceleration of gravity g [LT^{-2}]. Finally, $S_F = \tau_b/\rho g H$ is the friction slope for which an external closure relationship is required, i.e.,

$$S_F = \frac{n^2 U^2}{H^{4/3}}, \tag{5}$$

in the case where the Manning's resistance formula is adopted, where n is the roughness coefficient [$TL^{-1/3}$], or

$$S_F = \frac{C_F U^2}{gH}, \tag{6}$$

if the more physically based dimensionless bed resistance coefficient $C_F = \tau_b/\rho U^2$ is preferred, whose estimation can be obtained with the aid of the Keulegan (1938) relationship. Here, τ_b is the boundary shear stress [$ML^{-1}T^{-2}$], ρ is the water density [ML^{-3}], and $U = Q/A$ is the mean cross-sectional flow velocity [LT^{-1}].

The set of Eqs. (1)—(3) must be supplemented with appropriate initial and boundary conditions to obtain a unique problem solution and explicitly introduce the interacting flux D in Eq. (1) through a source term. Alternatively, the flux D can be brought directly into play by applying the 2D divergence theorem to Eq. (1). By doing so, under the assumptions of steady state flow and a no-flow boundary on the external portion of ∂Ω whenever its internal counterpart Γ concentrates the flux exchange dynamics (Fig. 1), the following simple integral form is obtained:

$$-\int_\Gamma \mathbf{n} \cdot T_r \nabla \Phi \, dS = \int_\Omega R \, d\Omega. \tag{7}$$

Here, $\mathbf{n}$ denotes the unit vector on Γ, which can have opposite directions after introducing a slit along Γ in order to make the boundary of Ω a simple closed curve (Fig. 2). Then, and within the bounds of the Dupuit—Forchheimer hypothesis (Fig. 2), the ambiguity in defining the direction of $\mathbf{n}$ is irrelevant as long as the integrand of the line integral above is recognized as the exchange flux $-T_r \partial\Phi/\partial n = D$, with D computed with Eq. (4). Here, the letter n indicating the directional derivative in normal direction should not be confused with the Manning's roughness coefficient. If it is now further assumed that D and R are constant, Eq. (7) reduces to the elementary mass balance

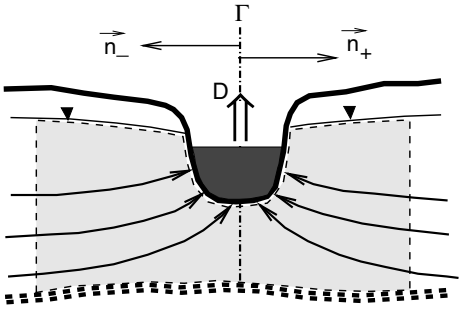

Figure 2 Total flow crossing the control volume from left and right adding to D.

$$D = \frac{R\Omega}{L_x}, \tag{8}$$

which states the trivial fact that the ultimate goal of an open ditch of length L_x is to drain all infiltrated irrigation water in excess of root uptake, evaporation, and soil pore water to reach field capacity. This result is used next to set up the simplified closed solution to the interacting drain—aquifer flow problem.

Simplified analytical solution

In order to give ground to the numerical test used to validate the iterative coupling between HEC-RAS and MODFLOW, it is sufficient to consider the steady-state solution to the groundwater discharge problem of an idealized, homogeneous aquifer defined on $0 < X < L_x$, $0 < Y < L_y$, bordered on one side by a fully penetrating channel drain with an uniform rectangular cross-section of width B, running in the X direction only and whose sloping bed obeys $Z_b = Z_{b_o} - S_o X$ (Fig. 3). To that aim, it is convenient first to introduce dimensionless variables as follows:

$$(x, y, z,\ h, \phi) = \frac{(X, Y, Z, H, \Phi)}{B}, \quad t = \frac{TV}{B}, \quad t_r = \frac{T_r}{KB}, \quad u = \frac{U}{V}, \tag{9}$$

where K is the hydraulic conductivity [LT^{-1}] of the aquifer and V is a velocity scale [LT^{-1}] given by

$$V = (gS_o D/C_F)^{1/3}. \tag{10}$$

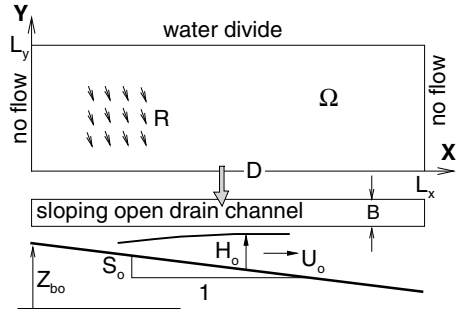

Figure 3 Layout of the test case. Only the upper part of the aquifer is sketched here, the other half extents from $Y = 0$ to $Y = -L_y$.

Then, the dimensionless form of the governing Eqs. (1)–(3) becomes

$$\varepsilon^{-1}\frac{\partial\phi}{\partial t} - \left[\frac{\partial}{\partial x}\left(t_r\frac{\partial\phi}{\partial x}\right) + \frac{\partial}{\partial y}\left(t_r\frac{\partial\phi}{\partial y}\right)\right] = r, \tag{11}$$

$$\frac{\partial h}{\partial t} + \frac{\partial(uh)}{\partial x} = \sigma, \tag{12}$$

$$\frac{\partial u}{\partial t} + u\frac{\partial u}{\partial x} + \mathrm{F_B}^{-2}\frac{\partial h}{\partial x} = \mathrm{F_B}^{-2}S_o - \mathrm{C_F}\frac{u^2}{h} - \sigma\frac{u}{h}, \tag{13}$$

whereas the dimensionless parameters are given by

$$\varepsilon = \frac{K}{S_y V}, \quad r = \frac{R}{K}, \quad \sigma = \frac{D}{VB}, \quad \lambda = \frac{\Lambda}{K}, \quad \mathrm{F_B} = \frac{V}{\sqrt{gB}}, \tag{14}$$

where $\mathrm{F_B}$ could be associated with the Froude number, albeit without any dynamical significance. A discussion in terms of the actual Froude number is given after describing the analytical solution to the posed problem. Now, if the variation in x direction in Eq. (11) under a steady constant drain flow discharging into the open channel, and the inertia, pressure, and momentum deficit due to the lateral influx on Eq. (13) are all assumed negligible, the reduced problem termed normal flow, hereafter referred with an ''o'' subscript is written from Eqs. (11)–(13), and Eqs. (4) and (7), as

$$\frac{\mathrm{d}}{\mathrm{d}y}\left(t_r\frac{\mathrm{d}\phi_o}{\mathrm{d}y}\right) \cong -r, \tag{15}$$

$$\frac{\mathrm{d}}{\mathrm{d}x}(u_o h_o) = \sigma, \tag{16}$$

$$\mathrm{F_B}^{-2}S_o - \mathrm{C}_{F_o}\frac{u_o^2}{h_o} \cong 0 \tag{17}$$

subject to

$$\left(t_r\frac{\mathrm{d}\phi_o}{\mathrm{d}y}\right)_{y=0} = \lambda\,[\phi_o(0) - (h_o(x) + z_b(x))], \tag{18}$$

$$\left(t_r\frac{\mathrm{d}\phi_o}{\mathrm{d}y}\right)_{y=l_y} = 0, \tag{19}$$

$$(u_o h_o)_{x=0} = 0. \tag{20}$$

Eq. (15) is readily solved for the linear case, t_r = const., and for the nonlinear case, $t_r = \phi_o$ (Bear, 1972), as well, whereas Eqs. (16) and (17) are simply solved by direct integration

$$\phi(y;x) = h_o(x) + z_b(x) + \frac{rl_y}{\lambda} + \frac{rl_y}{2t_r}y\left(2 - \frac{y}{l_y}\right), \tag{21}$$

$$\phi(y;x) = \sqrt{\left(h_o(x) + z_b(x) + \frac{rl_y}{\lambda}\right)^2 + rl_y y\left(2 - \frac{y}{l_y}\right)}, \tag{22}$$

$$h_o(x) = \sigma x^{2/3}, \tag{23}$$

$$u_o(x) = x^{1/3}, \tag{24}$$

where the parametric dependence of ϕ with x comes through the variation of the water surface elevation along the channel drain. Eqs. (23) and (24) were obtained by Woolhiser and Liggett (1967) with classical overland flow theory, adapted here to the drain flow problem. Eqs. (16) and (17) represent the time-independent kinematic wave approximation of Lighthill and Whitham (1955) to the full equations of motion.

The solution of Woolhiser and Liggett (1967), i.e., Eqs. (23) and (24), can be recast in dimensional form as follows:

$$\mathrm{F}_o^2 = \frac{U_o^2(X)}{gH_o(X)} = \frac{S_o}{\mathrm{C}_{F_o}}, \tag{25}$$

which represents a strict balance between bed resistance and gravity, i.e., whereas an increase in S_o tends to accelerate the flow, an increase in C_{F_o} will have the opposite effect. Based on the normal flow solution, the Froude number F_o represents an invariant quantity of the motion. The relation between F_B and F_o is therefore

$$\mathrm{F}_o^2 = \mathrm{F_B^2}\frac{u_o^2(x)}{h_o(x)} = \frac{\mathrm{F_B^2}}{\sigma}. \tag{26}$$

Using Manning's resistance relationship, i.e., Eq. (5) instead of Eq. (6), the normal flow solution would have the form

$$H_{o,n}(X) = \left(\frac{nD}{\sqrt{S_o}}\frac{X}{B}\right)^{3/5}, \quad U_{o,n}(X) = \left(\frac{\sqrt{S_o}}{n}\right)^{3/5}\left(\frac{DX}{B}\right)^{2/5}, \tag{27}$$

under the assumption that $H_o/B \ll 1$, in which case the hydraulic radius is well approximated by the local water depth. Knowing the value of one resistance coefficient, the corresponding value of the other can be computed with $\mathrm{C_F} = gB^{1/5}Q_{\mathrm{out}}^{-1/5}n^{9/5}(S_o/0.216)^{1/10}$, where, according to Eq. (8), $Q_{\mathrm{out}} = D\,L_x$.

Numerical solution with HEC-RAS/MODFLOW

The HEC-RAS code

HEC-RAS is a public domain code developed by the US Army Corp of Engineers (USACE, 2002). It performs 1D steady and unsteady flow calculations on a network of natural or man-made open channels. Basic input data required by the model include the channel network connectivity, cross-section geometry, reach lengths, energy loss coefficients, stream junctions information and hydraulic structures data. Cross-sections are required at representative locations throughout a stream reach and at locations where changes in discharge, slope, shape or roughness occur. Boundary conditions are necessary to define the starting water depth at the stream system endpoints, i.e., upstream and downstream. Water

surface profile computations begin upstream for subcritical flow or downstream for supercritical flow. Discharge information is required at each cross-section in order to compute the water surface profile. If the momentum deficit due to the lateral inflow D is ignored, the non-conservation form of the governing equations, under a steady flow assumption, i.e., Eqs. (2) and (3), can be integrated between an upstream and a downstream cross-section as

$$\int_1^2 \mathrm{d}Q = \int_1^2 D\,\mathrm{d}S, \tag{28}$$

$$\int_1^2 \mathrm{d}\left(Z_b + H + \alpha\frac{U^2}{2g}\right) = -\int_1^2 S_F\,\mathrm{d}S, \tag{29}$$

where α is a momentum correction factor usually set equal to one. HEC-RAS solves the resulting integral expressions of these simple equations by means of an iterative procedure called the standard step method. The right-hand side of Eq. (29) includes contraction or expansion losses as well as bed resistance losses through an average friction slope between the two consecutive cross-sections, the later based on the Manning roughness coefficient. Further details may be found in the HEC-RAS documentation manual (USACE, 2002).

The MODFLOW code

A full description of MODFLOW capabilities can be found in McDonald and Harbaugh (1988) and Harbaugh et al. (2000). For the purpose of this work, it is pertinent to revise some definitions introduced in MODFLOW to compute drain flows or exchange flows, with the understanding that in the latter case only groundwater discharge toward drains is considered in this work. Nonetheless, the approach is general enough to be applied to exchange flows in both directions. From Eq. (28), for D = const., groundwater discharge toward a channel drain contained within a MODFLOW cell of size ΔS is just $\Delta Q = D\Delta S$, where ΔS can either represent ''delr'' or ''delc'' according to MODFLOW cell size definition (McDonald and Harbaugh, 1988). Invoking now the constitutive relationship that defines drain flow, i.e., Eq. (4), the following equivalences between parameters used in MODFLOW and those introduced in this work are obtained:

$$\Delta Q = C_s[\Phi - (H + Z_b)], \tag{30}$$

$$C_s = \Lambda\Delta S = K_s\Delta S B/e_s, \tag{31}$$

where C_s is the hydraulic conductance of the channel drain–aquifer interface [L^2T^{-1}], K_s is the hydraulic conductivity of the streambed material [LT^{-1}], and e_s is the thickness of the streambed layer [L]. From these definitions, the hydraulic impedance of the channel–aquifer interface is defined as $\Lambda^{-1} = e_s/K_sB$ [TL^{-1}].

Picard iterates to couple HEC-RAS with MODFLOW

The system of Eqs. (1)–(4) can be solved with a sequence of approximations called Picard iterates. The computation begins with a crude approximation to the water depth distribution along the drain channel, namely an initial constant function $H^{(0)} = H^{(0)}(S)$. Then, a solution $\Phi^{(1)} = \Phi(\boldsymbol{X}, H^{(0)})$ is computed with MODFLOW to obtain a first estimate of drain flows, $D^{(1)} = D(S;\Phi^{(1)}, H^{(0)})$. It follows that, in order to obtain an improved approximation to the water elevation distribution on the channel drain, a first Picard iterate is computed with HEC-RAS, namely $H^{(1)} = H(S;D^{(1)})$. If the procedure is then repeated, a new approximation to the aquifer head $\Phi^{(2)} = \Phi(\boldsymbol{X}, H^{(1)})$ is obtained, which in turn, produces a second Picard iterate for drain flows, $D^{(2)} = D(S;\Phi^{(2)}, H^{(1)})$. The expectation is that, under suitable conditions, the Picard iterates $H^{(k)}$ and $\Phi^{(k)}$ converge to the exact solution of the system (1)–(3) as (k) grows. In practical terms, one or two iterates suffice to reach convergence within some prescribed tolerance, as illustrated next. The iterative scheme can be algorithmically posed as follows:

$$\begin{aligned}
&\text{Step 1}: \text{(a) Set } k=0, \text{and fix } H^{(k)} \text{ on } \Gamma,\\
&\quad\ : \text{(b) Solve for } \Phi^{(k+1)} = \Phi(\boldsymbol{X}, H^{(k)}) \text{ on } \Omega,\\
&\quad\ : \text{(c) Compute } D^{(k+1)} = D(S;\Phi^{(k+1)}, H^{(k)}) \text{ on } \Gamma,\\
&\text{Step 2}: \text{(a) Fix } D^{(k+1)} = D(S;\Phi^{(k+1)}, H^{(k)}) \text{ on } \Gamma,\\
&\quad\ : \text{(b) Compute } H^{(k+1)} = H^{(k+1)}(S;D^{(k+1)}) \text{ on } \Gamma,\\
&\text{Step 3}: \text{(a) If } \left(\left\|H^{(k+1)} - H^{(k)}\right\| / \left\|H^{(k+1)}\right\|\right) < tol \rightarrow \text{ end},\\
&\quad\ : \text{(b) Otherwise set } k = k+1, \text{ and return to (1b)}
\end{aligned} \tag{32}$$

Above, the norm $\|\cdot\|$ adopted during the computations represents the sum of the absolute values of all water depths defined along Γ.

Numerical solution

First, the solution to the hypothetical stream–aquifer interaction problem sketched in Fig. 3 and approximated by Eqs. (21)–(24), and (27), was computed with a channel drain running from west to east along the aquifer centre. The aquifer was symmetric with respect to the drain, with dimensions $L_x = 5000$ m and $L_y = 1260$ m. Channel drain parameters were $B = 5$ m, bed elevation at the channel headwater $Z_{b_o} = 22$ m, $S_o = 4\times10^{-4}$, and $n = 0.05$. This value of Manning's roughness coefficient can be associated with the resistance encountered in not-well maintained channels colonized by weeds on their banks, a situation that resembles the drainage system of a real case application discussed later. In addition, for a drain flow per unit length of channel $D = 2\times10^{-4}$ m^2 s^{-1}, and a net recharge to the aquifer $R = 7.936508\times10^{-8}$ m s^{-1}, it follows from Eq. (8) that the total outflow at the channel drain endpoint is $Q_{out} = DL_x$ ($=R\Omega$) = 1 m^3 s^{-1}. Other parameter values used for the test were $T_r = 0.014$ m^2 s^{-1}, $K = 7\times10^{-4}$ m s^{-1}, and $\Lambda = 0.2$ m s^{-1}. The associated dimensionless parameters and the velocity scale were: $t_r = 4$, $r = 1.1338\times10^{-4}$, $\lambda = 285.71$, $\sigma = 1.3887\times10^{-3}$, $F_B = 0.0041$, $F_o = 0.11$, $C_F = 0.03284$, and $v = 0.03$ m s^{-1}. A 3D view of the solution to the hypothetical stream–aquifer interaction problem defined by Eqs. (22) and (23) for these parameter values is depicted in Fig. 4, where the channel width was exaggerated for illustration purposes. Now, if D = const., Eqs. (2) and (3) become uncoupled from Eq. (1), and the governing Eqs. (28) and (29) can be solved independently by HEC-RAS. Thus, the sensitivity of the model output to variations

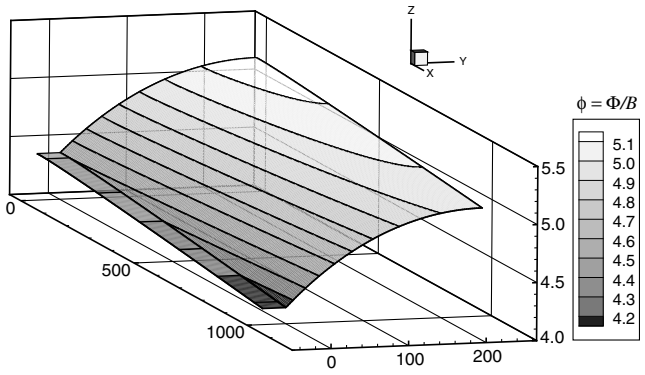

Figure 4 3D view of the coupled stream–aquifer solution given by Eqs. (22) and (23).

in some input parameters such as the grid size and the inflow rate at the upstream end of the channel can be tested without resorting to the fully coupled problem.

Initially, the channel length was discretized into 51 rectangular cross-sections evenly spaced every 100 m. A lateral inflow $\Delta Q = D\Delta S = 0.02\ m^3\ s^{-1}$ was added at the upstream cross-section of each simulated channel reach. In agreement with Eq. (17), the condition $S_F = S_o$ was imposed at the downstream boundary. Analytical solutions and computed results are depicted in Fig. 5. It is seen that the normal flow solution predicted by Eq. (23) closely follows the solution given by Eq. (27) which, in turn, was made dimensionless against B. The value of C_F used for the curve shown in Fig. 5 was obtained with the expression given at the end of Simplified analytical solution, for $n = 0.05$ and $Q_{out} = 1\ m^3\ s^{-1}$. The excellent agreement between the solid line (Manning's n) and the dash–dot line (Keulegan's C_F) indicates that in-channel water depth computations are quite insensitive to the type of hydraulic resistance law. On the other hand, a slight departure or overshoot in the computed free surface is clearly noticeable in Fig. 5. Part of the problem is originated by the fact that the upstream boundary condition given by Eq. (20) cannot be exactly replicated by HEC-RAS. In other words, the integral form of Eq. (28), $Q_2 = Q_1 + D\Delta S$, requires a non-trivial inflow value Q_1 at the uppermost stream cross-section. Consequently, a hypothetical inflow rate equal to $0.00025\ m^3\ s^{-1}$ was imposed at that location, which was gradually reduced as far as possible in successive simulations to approach zero. The final value for the simulations was $0.0001\ m^3\ s^{-1}$. For smaller values, HEC-RAS reported a zero-flow error message. For upstream inflow rates of 0.0001 and $0.00025\ m^3\ s^{-1}$ the water depth computed at the channel headwater was 0.06 and 0.07 m, respectively. Similar results were also obtained with a coarser grid of 21 cross-sections. After uniformly subtracting the initial overshoot, the consistency between numerical results and the theoretical water profile distribution is shown in Fig. 5. As explained, the approximately constant overshoot on the computed free surface is in part triggered by the inadequacy of HEC-RAS in handling a null water depth at the inlet, though a fraction of it could be attributed to the dynamic response of the full equation of motion embedded into the solution. The normal flow solution discussed earlier is strictly based upon the kinematic wave approximation. Nevertheless, if the normal flow solution itself is used to evaluate the relevance of the neglected terms into the balance of forces, i.e., inertia, pressure, and momentum deficit, with respect to the retained terms, i.e., gravity and friction, it is rather straightforward to determine that the weight of the neglected terms decays very rapidly with $x^{-1/3}$. In summary, HEC-RAS capabilities and accuracy to reproduce the essential features of the normal flow solution discussed up to here were deemed acceptable for the purpose of this work, given the fact that the slight overshooting of the computed water depth introduces a rather small variation into the computed flux exchange D, as explained next.

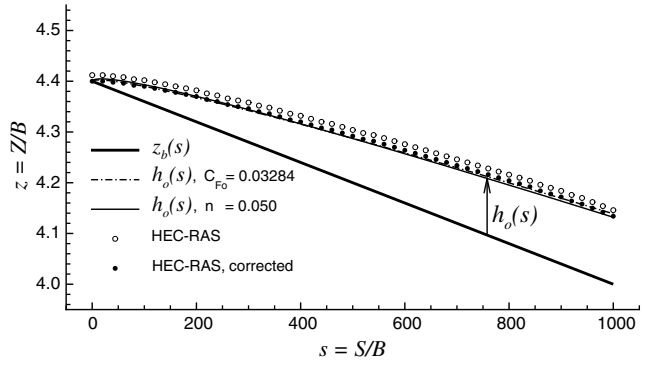

Figure 5 Comparison between computed $h_o(x)$ with HEC-RAS, for D = const., and analytical distributions obtained for both bed resistance relations discussed in this work.

The approximate analytical solutions given by Eqs. (21), (22) and (27) were then compared with the numerical results obtained when HEC-RAS and MODFLOW were iteratively coupled following the algorithm (32). The MODFLOW grid consisted of 20 columns 250 m wide ($m_x = 20$) and 21 rows 120 m wide ($m_y = 21$). The drain channel was located along the centre row ($i = 11$) and represented by 20 MODFLOW drain cells. HEC-RAS channel discretization amounted for 21 rectangular cross-sections located at the boundary between two contiguous MODFLOW drain cells, except for the first and last ones. Therefore, they were staggered with the centre of MODFLOW drain cells. The exact value of the groundwater flow discharging from each MODFLOW cell into the channel drain, computed from Eq. (30), was $\Delta Q = D\Delta X(= Q_{out}/m_x) = 0.05\ m^3\ s^{-1}$. The hydraulic conductance of the channel–aquifer interface, C_s, was equal to $50\ m^2\ s^{-1}$. From Eq. (31), it follows that this value of C_s corresponds to a hydraulic conductivity of the streambed material of $0.04\ m\ s^{-1}$, for a streambed layer thickness of 1 m. The aquifer bottom was made coincident with the datum, set equal to zero, while the aquifer top was set equal to 25 m. MODFLOW computations were first restricted to the linear- or confined-aquifer case. Fig. 6 shows the Picard iterates of the water surface profiles computed with HEC-RAS, starting from an initial guess $H^{(0)} = 0.30$ m. Each HEC-RAS computation was obtained after passing onto each of the channel reaches the cumulative drain flow computed by MODFLOW. The first and second Picard iterates are practically indistinguishable to the naked eye, obtained after imposing upstream and downstream boundary conditions as previously discussed. The corresponding water depth calculated at $X = 0$ m was 0.07 m. The overshoot is

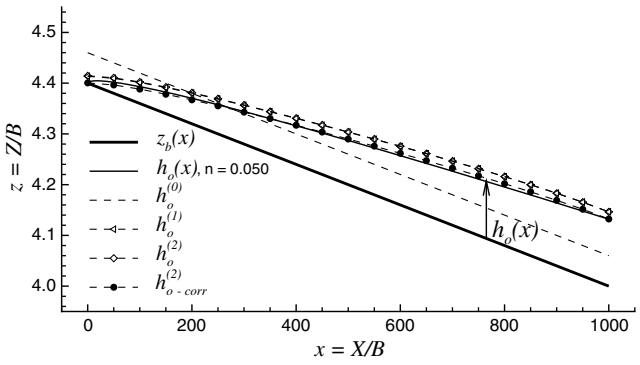

Figure 6 Variation of the Picard iterates $h^{(k)}$ obtained after coupling HEC-RAS with MODFLOW HEC-RAS solutions were obtained by accumulating the value of $D^{(k+1)}(\boldsymbol{X};\Phi^{(k+1)},H^{(k)})$. along drain channel reaches.

systematically propagated in a more or less constant manner in the downstream direction. It can be seen in Fig. 6 that once that overshoot is subtracted from the Picard second iterate, the computed water surface profile closely resembles the normal flow solution given by Eq. (27). For each Picard iteration, the steady-state MODFLOW simulation started from a constant initial aquifer head equal to 25 m. The groundwater flow simulation required, on average, 11 iterations to converge using a head closure criterion of 0.0001 m and the Strongly Implicit Procedure-SIP solver. The cell drain flux values computed with MODFLOW for all Picard iterates as well as their relative error expressed in percentage are plotted in Fig. 7. An end-effect is clearly present at both ends of the drain channel. One way to eliminate this effect is by locally averaging the flux within neighbouring cells, since the average flux is quite close to the exact value (see Table 1). Both, cell values as computed by MODFLOW (Fig. 7) and their average were used without any noticeable difference in the final solution. The evolution of the error closure criteria for the in-channel water depth results, along with the average exchange flux computed by MODFLOW, are given in Table 1. Here, the error tolerance mentioned in the three-step algorithm (32) was fixed at 0.01 and the overall mass balance error reported by MODFLOW was less than 0.1%.

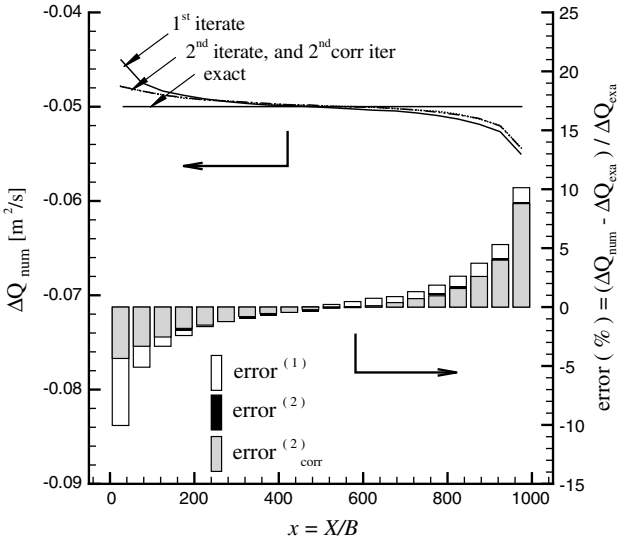

Figure 7 Cell drain flux values as computed by MODFLOW — error distribution of the computed flux, in percentage.

Table 1 Evolution of the average drain flux computed by MODFLOW (minus sign obeys convention) and the in-channel water depth error calculated by HEC-RAS

Picard iterate	1st	2nd	Corrected
$\frac{\sum \Delta Q_j}{m_x}$ ($m^3\ s^{-1}$)	−0.0500575	−0.0500580	−0.0500530
$\frac{\sum \lvert H_j^{(k+1)} - H_j^{(k)} \rvert}{\sum \lvert H_j^{(k+1)} \rvert}$	0.4819561	0.0045554	

Aquifer head contours computed with MODFLOW were compared with those obtained with Eq. (22) in Fig. 8 for a nonlinear (unconfined) aquifer case. For the linear case, the results are similar and were omitted here for the sake

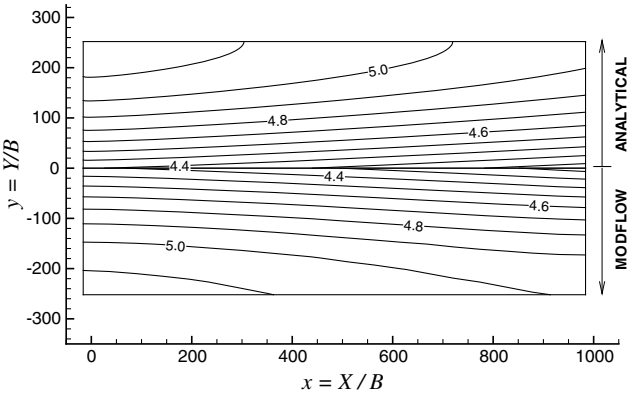

Figure 8 Contour lines of the dimensionless aquifer head, nonlinear case. (upper half) Approximate analytical solution given by Eq. (22). (lower half) Solution computed by MODFLOW.

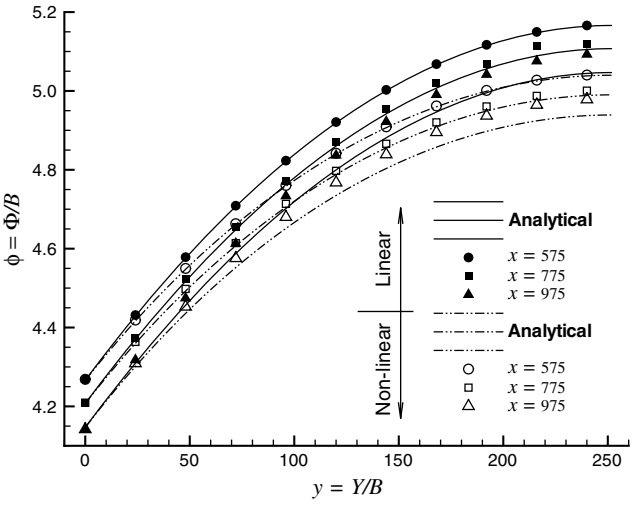

Figure 9 Comparison between the approximated analytical solutions and the results computed with MODFLOW of the aquifer head profiles in the *y* direction for *x* = const.

of brevity. Actually, three transverse aquifer profiles at selected x positions are shown in Fig. 9 for both, linear and nonlinear cases. The matching degrades as x increases, preserving a remarkable fit throughout the domain close to the channel boundary, where drain fluxes are computed. Part of the discrepancies were triggered by the conditions MODFLOW must meet at the no-flow boundary at $Y = L_y$ given the coarseness of the grid used. A better agreement at the boundary was obtained with a finer grid composed by $m_x = 50$ columns and $m_y = 41$ rows, matching the HEC-RAS calculations depicted in Fig. 5. Nevertheless, exchange fluxes obtained with the finer grid were essentially indistinguishable from fluxes obtained with the coarser grid plotted in Fig. 7, therefore the results could be considered grid-size independent from a flux perspective. Obtaining similar results with different grids and validating the calculations between HEC-RAS and MODFLOW against analytical solutions with a grid size similar to the grid used later on a real case application were considered an essential aspect of the study.

Model sensitivity

Unfortunately, the approximate analytical solution defined by Eqs. (21)–(24), and (27) is not very useful to explore model sensitivity, as it will become clear in a moment. HEC-RAS is known to be sensitive to channel width B and, to a lesser extent, to the roughness coefficient n, whereas MODFLOW is not very sensitive to the hydraulic conductance that controls the exchange flux $\Delta Q = D\Delta S$ (Chen and Chen, 2003). The stiffness of the groundwater model response to changes in the hydraulic conductance can be understood from Eq. (8). This equation shows that the exchange flux is indeed independent of any groundwater model parameter, unless the hydraulic conductance is regionally variable, in which case the mass balance reads $\int_\Gamma D dS = R\Omega$. The exchange flux ΔQ given by Eq. (30) is considered the quantity of interest for the proposed approach. Consequently, in order to analyze changes in ΔQ with respect to the base state or normal flow condition studied before, caused by changes in the hydraulic conductance, a set of simple numerical experiments were run with a fixed in-channel water surface (i.e., the corrected water depth depicted in Fig. 6). Then, the hydraulic conductance on the upper half of the drain channel was reduced one order of magnitude on each simulation, whereas the lower half always preserved the originally assigned value of $50\ m^2\ s^{-1}$. Since the computed solution developed an increasing dependence with X for decreasing values of C_s on the upper half of the drain, the approximate analytical solution was not helpful. Nevertheless, from elementary differential calculus it is straightforward to establish that the net effect of a departure δC_s from the base state C_s on the model output would be $\delta\Delta Q = \delta C_s\, \partial\Delta Q/\partial C_s$, expression that can be written in terms of the absolute value of the relative change as

$$\kappa = \frac{|\delta\Delta Q/\Delta Q_o|}{|\delta C_s/C_{s_o}|}, \tag{33}$$

which is known as the sensitivity coefficient or condition number in the jargon of numerical analysis. A model is said to be sensitive if $\kappa > 1$, neutral if $\kappa = 0$, and robust if $\kappa < 1$. The variation of the sensitivity coefficient as a function of C_s depicted in Fig. 10 diminishes in the upper half of the drain channel. The sensitivity coefficient was less than one for the whole range of values of C_s explored. The model was quite insensitive until small values of the hydraulic conductance were reached. For all practical purposes, and for the two smallest values of C_s shown in Fig. 10, the model behaves as if the upper half of the drain channel was clogged, discharging the whole recharge on the lower half of the drain at twice the rate in comparison with the base rate.

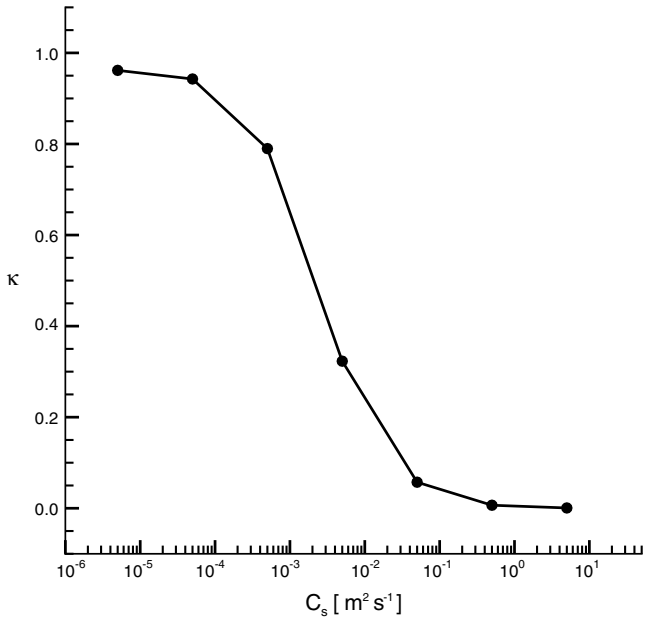

Figure 10 Variation of the sensitivity coefficient for decreasing values of the hydraulic conductance of the drain–aquifer interface.

Application to the Choele Choel Island, Patagonia, Argentina

The approach was applied to analyze the drainage problem of the shallow aquifer of the Choele Choel Island, located in the Patagonia region of Argentina. The Negro river, in the Argentinean Patagonia, originates at the confluence of the Neuquén and Limay rivers (Fig. 11). After traversing the Upper Valley, the Negro river enters the gently sloping Middle valley to continue through the Lower valley toward its outlet in the Atlantic Ocean. The Choele Choel Island lies at the bifurcation of the Negro river into its North and South branches. The island is approximately 40 km long with a maximum width of 15 km, and encompasses around 34,000 ha, including Chica Island and other small islets. The Choele Choel Island longitudinal slope is 5.8×10^{-4}. In the transverse direction, the island slopes gently from the South Branch toward the North Branch. Summer temperatures average 23 °C during January, while winter temperatures average 6.8 °C. Maximum temperatures of 30 °C are common in summer months. Below freezing temperatures occur in June, July, and August. The average annual precipitation is about 300 mm. Rainfall is unevenly distributed in

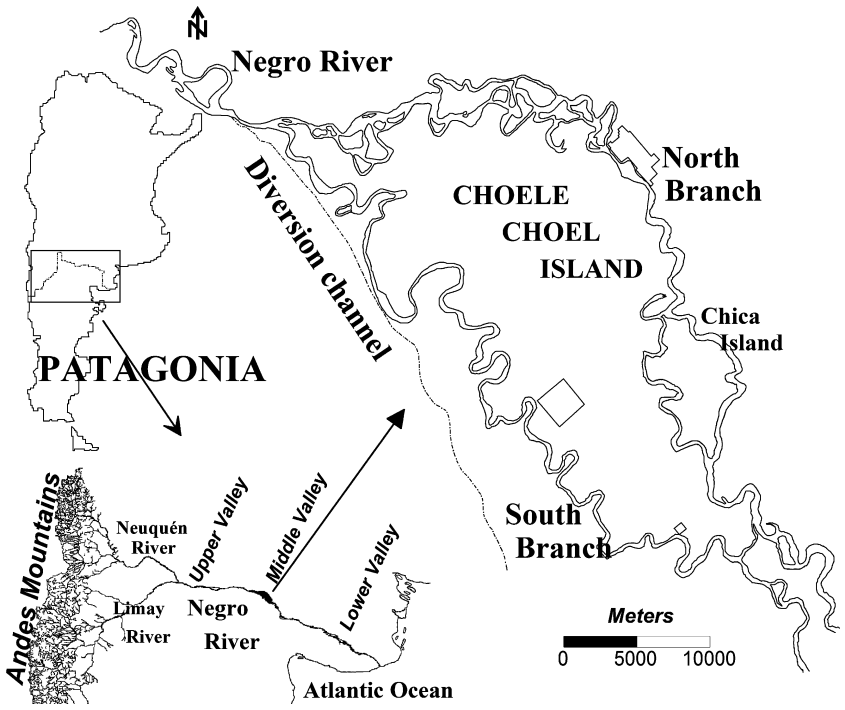

Figure 11 Study area.

space and time, as is typical in semiarid climates. The Middle Valley was carved in the Patagonian Plateau by glaciers. Three geologic units form the Valley's stratigraphic profile: (1) Negro river Formation (Rionegrense): the lowermost portion of the profile, composed by alternate layers of sand, silt, and clay of moderate to low permeability. Despite its thickness, it is of little hydrogeologic interest; (2) Rodados Patagónicos: composed of conglomerates and boulders, usually cemented with calcium carbonate. These beds vary in thickness from 3 to 5 m and extend over the terraces surrounding the valley; (3) Relleno Moderno: overlies the Rionegrense in the valley centre. It is mainly composed of a thin layer of silty sand, underlain by gravel deposits with variable quantities of sand, and is characterized by high permeability. This is the main water-bearing unit of the profile. Unconfined in most of the area, it is highly dynamic and interacts closely with all surface water sources and sinks. Transmissivity values for this aquifer range from 200 to 2500 m^2 day^{-1}, while reported values for specific yield vary between 0.01 and 0.2. Field studies have shown that there is no hydraulic connection between the Relleno Moderno and the underlying formation. The North Branch conducts more than 90% of the upstream flow. Both branches act as natural drainage canals, providing over 155 km of stream—aquifer contact that allows free groundwater drainage. The South Branch is a highly meandering stream approximately 87 km long, while the North Branch is 68 km long.

The local economy is based on the production of fruits and vegetables, sustained by an irrigation/drainage system. Irrigation water enters the island through an unlined 19 km long channel, starting at the western corner of the island, 3.5 km downstream from the bifurcation point in the Negro river branches. Eight secondary, unlined channels 89.8 km long, and minor channels that reach outlying irrigated fields (61.2 km long) complete the irrigation network. Irrigation is by gravity, with an application frequency of about two to three weeks, on average. Natural drainage is supplemented by about 100 km of drain canals of different sizes that remove excess water accumulated during the irrigation season. Drainage water is then discharged at downstream locations at both river branches. Small canals are usually poorly maintained, silted up and colonized by weeds, while major canals are periodically dredged. Fig. 12 shows the configuration of the drainage network.

During the irrigation season, which extends from late August to early April, seepage losses through unlined distribution canals and in irrigated fields cause water table mounding and/or soil water logging at some locations. Moreover, high stream levels caused by high water releases for hydroelectric power generation at upstream dams during the peak of the irrigation season interfere with free groundwater drainage causing backwater effects at some drainage canals discharge points.

MODFLOW — HEC-RAS set up

MODFLOW was implemented to simulate steady-state groundwater flow in the island during the non-irrigation season, when only drainage canals and streams are active. This simulation provided the first set of drain flows later used as lateral inflows to HEC-RAS. The finite difference grid contained 134 rows and 64 columns, oriented along the regional groundwater flow direction, with a regular cell size of 300 m. A single model layer, 20 m thick, representing the unconfined Relleno Moderno was simulated. More details regarding the model set-up and calibration results can be found in Rodríguez et al. (2006)); only drain related parameters and results are summarized here for the purpose of this work.

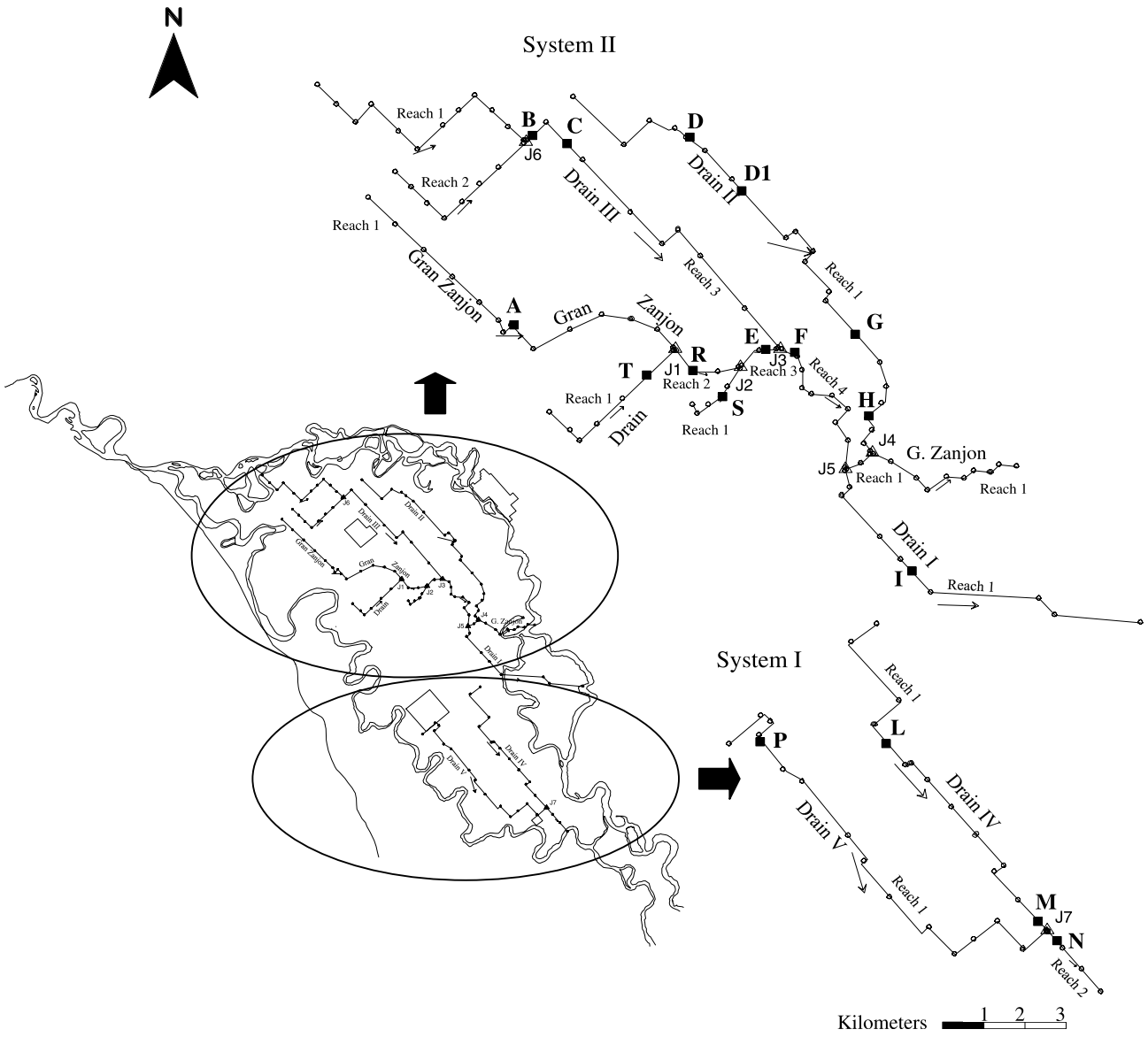

Figure 12 Drain channels network of the Choele Choel Island, location of field data points.

The drainage system shown in Fig. 12 was simulated with 324 drain cells according to the DRN Package input requirements. The so-called System I drains the Southeastern portion of the island and discharges into the South Branch of the Negro river, System II drains the North-western and central portions of the island and discharges into the North Branch of the Negro river. Water depth data for drain channels were available only at a few locations, hence it was necessary to estimate initial values in order to implement the DRN Package. Based on previous knowledge of the site and those few data points, water depth at drain channels headwaters was assumed to be about 0.2—0.3 m. These depths were progressively increased downstream until a water depth of 1.80, 0.9, and 1.14 m was reached at discharge points of Drain IV, Drain I and the Gran Zanjón, respectively (see Fig. 12 for their location). Continuity of water levels between stream channels and discharging drain channels was preserved at discharge points. The stage at the receiving stream was estimated by interpolating stream height readings from gauging stations located upstream and downstream of the discharge points.

Calibrated values for drain conductance ranged from 0.003 to 0.0068 $m^2 s^{-1}$. The total simulated drain flow was 0.726 $m^3 s^{-1}$, of which 0.247 $m^3 s^{-1}$ (34%) were drained by System I and 0.479 $m^3 s^{-1}$ (66%) by System II. Not much information existed to assess the model performance regarding the magnitude and distribution of drain flows. However, agricultural engineers working at the site have roughly estimated a total drainage flow around 0.80 $m^3 s^{-1}$ for the non-irrigation season. Therefore, using this estimate, simulated drain flows were underestimated by roughly 9.25%.

A total of 101.25 km of drain canals were simulated with HEC-RAS. The network was discretized with 535 cross-sections distributed according to the hierarchy of drain channels, bottom slope, observed changes in cross-sections as well as HEC-RAS computational requirements to warrant the energy balance for the calculation of water depths

between two consecutive cross-sections. The bottom slope was obtained from topographic data, whereas all cross-sections were assumed rectangular-shaped. Channel widths were assigned based upon the analysis of photographs taken at the site and field surveys at selected locations. Due to deficient maintenance, flow conveyance is significantly reduced by weeds colonies and other plants at some locations, mainly in upstream reaches of drain channels. These conditions prevail along some reaches of Drain II and the Gran Zanjón. Following the description of channel characteristics given by Chow (1959), a Manning's roughness coefficient of 0.07 was adopted for those reaches, while a value of 0.055 was used for the rest of the network.

Picard iterates scheme

As explained before, drain flows obtained with the DRN Package at each MODFLOW drain cell were integrated according to the HEC-RAS cross-sections distribution and converted to lateral flows to start up a HEC-RAS simulation, and hence, the iterative process. HEC-RAS calculations were performed under a subcritical flow regime, imposing water surface elevations at drain canals discharge points into both streams. Based upon stream height records for both branches of the Negro river, the water surface elevation at the last cross-section of the Gran Zanjón, Drain I and Reach 2, Drain IV was fixed at 122, 119.7, and 116.8 m, respectively, equivalent to water depths of 1.14, 0.9, and 1.8 m.

Following the algorithm of Eq. (32), convergence was reached at the end of the second Picard iterate for a prescribed tolerance of 0.03 m. Stream stages and stream–aquifer interaction fluxes along both river branches were unaffected by the implementation of the iterative process. However, minor local adjustments to the aquifer hydraulic conductivity were introduced at the end of the process for a fine-tuning calibration of aquifer heads adjacent to the drainage network. The total drain flow at the end of the iterative process was 0.8369 $m^3 s^{-1}$, 34% were drained by System I and 66% by System II. Simulated total drain flows overestimated previous calculations by agricultural engineers by 4.6%, compared to the 9.25% underestimation ob-

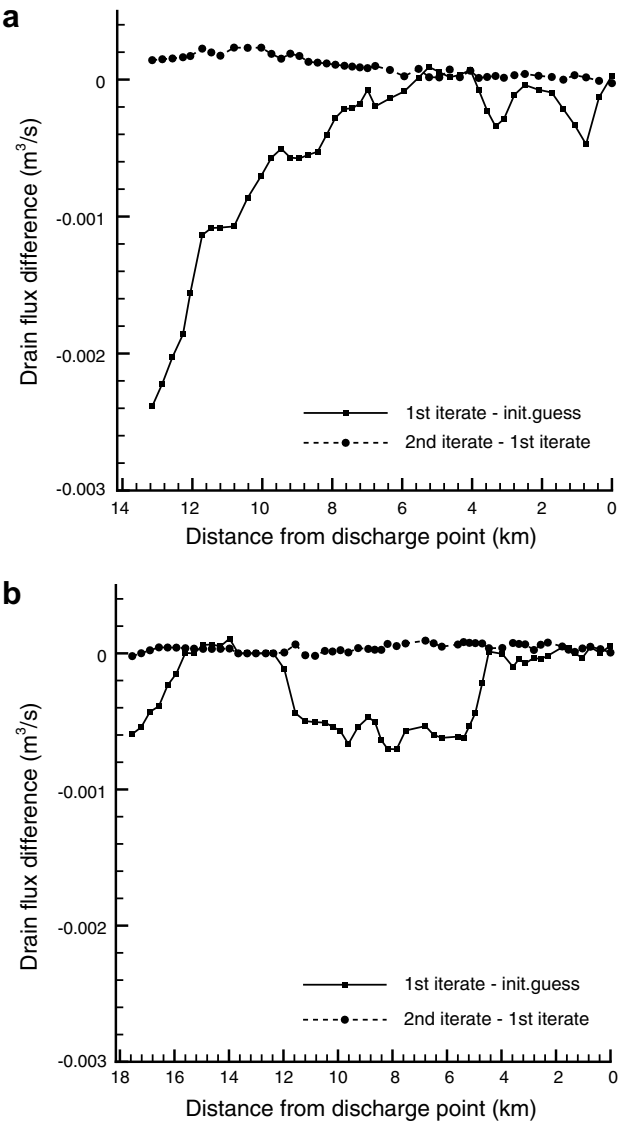

Figure 13 Drain flow differences between successive Picard iterates: (a) Drain V; (b) Gran Zanjón.

Table 2 Comparison between observed and simulated water depths and drain flows at selected points (see Fig. 12 for their location)

Location	Dist (m)	H_{obs} (m)	H_{sim} (m)	Err_H %	D_{obs} ($m^3 s^{-1}$)	D_{sim} ($m^3 s^{-1}$)	Err_D (%)
A	4858	0.22	0.16	27	0.024	0.03	25
R	1192	0.5	0.35	30			
F	3968	0.8	0.57	28	0.337	0.33	−2
D	11,362	0.3	0.21	30			
D1	9751	0.3	0.25	17	0.05	0.04	20
G	3866	0.55	0.24	50	0.065	0.05	23
H	1211	0.65	0.27	54			
B	9129	0.3	0.43	30			
C	7854	0.35	0.42	20	0.095	0.12	26
I	6147	0.9	0.67	25			
L	6611	0.4	0.2	50			
M	310	0.6	0.6	0			
N	1744	1	1.04	4			
P	11,196	0.25	0.28	12			

$Err_{H,D} = [H,D_{obs} - H,D_{sim}]/H,D_{obs}$. Dist, cumulative distance from the discharge point.

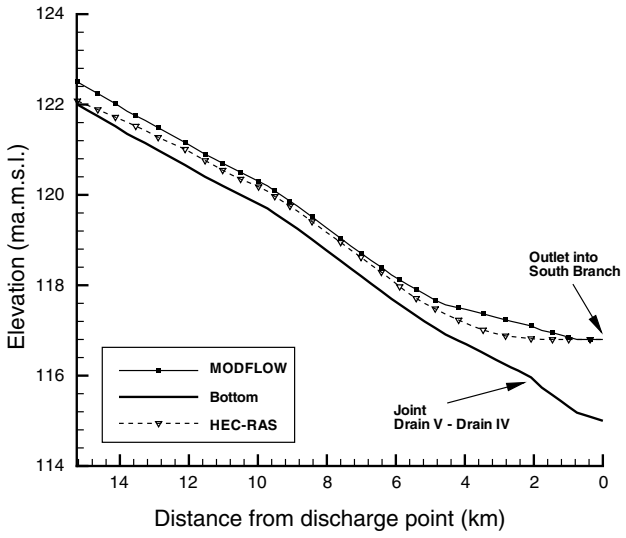

Figure 14 Simulated water surface profiles along Drain V–Reach 2 and Drain IV.

tained prior to the implementation of the Picard iterate procedure.

Table 2 contains water depth and channel discharge measured at selected points during the non-irrigation season (see Fig. 12 for points location) and corresponding simulated values. The application of the iterative modelling procedure was successful at reproducing drain flow patterns and water depths. Relative errors between observed and simulated drain flows fell between −2% and 26%. These values are considered satisfactory given the amount and quality of the field data available. On the other hand, simulated water depths with HEC-RAS were reasonably close to observed values, though in practical terms they were similar to the first guess input to MODFLOW DRN Package at check locations. In general, the errors between observed and simulated water depths were bracketed between 0% and 50%, with the best results obtained for Drains IV and V.

Fig. 13a illustrates the differences between drain flows along Drain V calculated at successive iterates. Cumulative distances are measured from the drain discharge point upstream. Even though changes between the 1st and 2nd iterates are very small, it is worth noting the differences between drain flows obtained with the first guess of water depths input to the DRN package and drain flows obtained after the 1st iterate. The greatest differences are mainly concentrated along a 5 km reach downstream from the drain headwaters, i.e., the reach where most of the uncertainly regarding drain channel information used to define initial MODFLOW drain heads was located. As indicated by the negative differences, drain flows obtained with the first guess were less than those obtained with water depths calculated with HEC-RAS. A similar analysis was repeated for the Gran Zanjón (Fig. 13b). In this case, the maximum differences were concentrated on a 2 km reach near the channel headwaters and along a 7 km reach located approximately at mid-distance between the channel endpoints. Similarly to Drain V, the first few kilometres entail great uncertainties due to the lack of field data. As for the mid-channel location along the Gran Zanjón, it is characterized by a non-straight reach, channel width changes and several junctions from smaller drain channels adding complexity to the simulation of the channel network.

Finally, Fig. 14 compares water surface profiles along Drain V-Reach 2 and Drain IV until its discharge into the South Branch for all Picard iterates. HEC-RAS gradually varying flow calculations improve the curvature of the hydraulic profile upstream and at the junction of Drain IV with Drain V.

Conclusions

Coupling public domain and standard models to extract the best of each individual model components is a modelling approach successfully pursued by many researchers. In this work HEC-RAS and MODFLOW have been iteratively coupled in an effort to improve the representation of hydraulic profiles in drain channels within a regional groundwater flow system. With the aid of a simple analytical solution, it was established that the proposed scheme is numerically convergent and mass conserving. That was accomplished by developing a simple approximate analytical solution for the coupling problem, which provided the mathematical setting for the proposed approach. Numerical results to the analytical solution obtained with a Picard iteration between HEC-RAS and MODFLOW were extensively analyzed.

The iterative process works as follows: drain flows resulting from a MODFLOW run with its DRAIN Package (DRN) driven by an initial guess of water depth on the drains become lateral flows input to HEC-RAS. Then HEC-RAS is run with appropriate geometric data to obtain a set of water depths in drain canals. This new water depths are introduced back into MODFLOW DRN Package for a new MODFLOW run, from which a new set of drain flows is obtained. These drain flows are input back into HEC-RAS as lateral flows and a new simulation is performed. Successive iterates are repeated until convergence, measured in terms of water depths, is achieved. The procedure was applied in the Choele Choel Island, Argentina, where scarce information regarding the drainage system obligated a tedious interpolation of few water depths to implement the MODFLOW DRN package. The approach not only provides a more sound hydraulic profile along drain canals for a wide range of downstream hydraulic conditions, but also could mean a considerable time saving in the burdensome task of specifying water depths along a large and complex drainage system with limited field data. It is recognized that this particular study was limited to the case of groundwater discharge to the surface water ant not the reverse, though the iterative procedure can be equally implemented for a stream/aquifer interaction scenario replacing the DRN package by the RIV package. Finally, the approach was developed under steady-state conditions, and therefore care should be exerted to extend the methodology to transient scenarios, in particular to handle different time scaling and potential HEC-RAS instabilities.

Acknowledgements

This material is based upon work supported in part by the Rio Negro State Water Authority, Universidad Nacional del Litoral, and Research Grant PICT 07-14721 of ANPCyT, all from Argentina, and by SAHRA (Sustainability of semi-Arid

Hydrology and Riparian Areas) under the STC Program of the National Science Foundation, Agreement No. EAR-9876800. The research was also supported in part by the Department of Hydrology and Water Resources of the University of Arizona. Thanks are also given to two anonymous reviewers that helped to improve the manuscript.

References

Banta, E.R., 2000. MODFLOW-2000, The US Geological Survey modular ground-water model. Documentation of packages for simulating evapotranspiration with a segmented function (ETS1) and drains with return flow (DRT1). Open-File Report 00-466.

Batelaan, O., De Smedt, F., 2004. SEEPAGE, a new MODFLOW DRAIN package. Groundwater 42 (4), 576–588.

Bear, J., 1972. Dynamics of Fluids in Porous Media. Dover, New York.

Carslaw, H.S., Jaeger, J.C., 1959. Conduction of Heat in Solids, 2nd ed. Oxford Science, 510 pp.

Chen, X., Chen, X., 2003. Sensitivity analysis and determination of streambed leakance and aquifer hydraulic properties. Journal of Hydrology 284, 270–284.

Chow, V.T., 1959. Open Channel Hydraulics. McGraw-Hill, New York.

Chow, V.T., Maidment, D., Mays, L.W., 1988. Applied Hydrology. McGraw-Hill, 572 pp.

Cooper, H.H., Rorabaugh, M.I., 1963. Ground-water movements and bank storage due to flood stages in surface streams. US Geological Survey Water Supply Paper, 343–366.

Hantush, M.M., 2005. Modelling stream–aquifer interactions with linear response functions. Journal of Hydrology 311, 59–79.

Harbaugh, A.W., Banta, E.R., Hill, M.C., McDonald, M.G., 2000. MODFLOW-2000, The US Geological Survey modular ground-water model — User guide to modularization concepts and the Ground-Water Flow Process: US Geological Survey Open-File Report 00-92, 121 pp.

Hogarth, W.L., Govindaraju, R.S., Parlange, J.Y., Koelliker, J.K., 1997. Linearized Boussinesq equation for modelling bank storage — a correction. Journal of Hydrology 198, 377–385.

Hunt, B., 1990. An approximation for the bank storage effect. Water Resources Research 26 (11), 2769–2775.

Hunt, B., 1999. Unsteady stream depletion from groundwater pumping. Ground Water 37, 98–102.

ILRI (International Institute for Land Reclamation and Improvement), 1994. Drainage principles and applications. In: Ritzema, H.P. (editor-in-Chief), ILRI Publication 16, 2nd ed. (Completely Revised), Wageningen, The Netherlands.

Jobson, H.E., Harbaugh, A.W., 1999. Modification to the diffusion analogy surface-water flow model (DAFLOW) for coupling to the modular finite-difference ground-water flow model (MODFLOW), US Geological Survey Open-File Report 99-217, 59 pp.

Johnson, M., Koenig, R., 2003. Solutions to soil problems. III. Drainage. AG/Soils/2003/03. Utah State University.

Keulegan, G.H., 1938. Laws of turbulent flow in open channels. National Bureau of Standards Research Paper RP 1151, USA.

Lighthill, M.J., Whitham, G.B., 1955. On kinematic waves. I. Flood movements in long rivers. Proceedings of the Royal Society of London, Series A 229 (1178), 281–316.

McDonald, M.G., Harbaugh, A.W., 1988. A modular three-dimensional finite difference ground-water flow model. US Geological Survey Techniques of Water-Resources Investigations, Book 6, Chapter A1, 586 pp.

Moench, A.F., Barlow, P.M., 2000. Aquifer response to stream-stage and recharge variations. I. Analytical step-response functions. Journal of Hydrology 230, 192–210.

Panday, S., Huyakorn, P.S., 2004. A fully coupled physically-based spatially distributed model for evaluating surface/subsurface flow. Advances in Water Resources 27, 361–382.

Parlange, J.-Y., Hogarth, W.L., Govindaraju, R.S., Parlange, M.B., Lockington, D., 2000. On an exact analytical solution of the Boussinesq equation. Transport in Porous Media 39, 339–345.

Pinder, G.F., Sauer, S.P., 1971. Numerical simulation of a flood wave modification due to bank storage effects. Water Resources Research 7 (1), 63–70.

Pohll, G.M., Guitjens, J.C., 1994. Modelling regional flow and flow to drains. Journal of Irrigation Drainage Engineering ASCE 120 (5), 71–82.

Prudic, D.E., 1989. Documentation of a computer program to simulate stream–aquifer relations using a modular, finite-difference, ground-water model. US Geological Survey Open-File Report 88-729, 113 pp.

Prudic, D.E., Konikow, L.E., Banta, E.R., 2004. A new streamflow-routing (SFR1) package to simulate stream-aquifer with MODFLOW 2000. US Geological Survey Open-File Report 2004-1042, 104 pp.

Rodríguez, L.B., Cello, P.A., Vionnet, C.A., 2006. Modelling stream–aquifer interactions in a shallow aquifer, Choele Choel Island, Patagonia, Argentina. Hydrogeology Journal 14, 591–602.

Serrano, S.E., Workman, S.R., 1998. Modelling transient stream/aquifer interaction with the non-linear Boussinesq and its analytical solution. Journal of Hydrology 206, 245–255.

Skaggs, R.W., Breve, M.A., Gilliam, J.W., 1995. Predicting effects of water table management of loss of nitrogen from poorly drained soils. European Journal of Agronomy 4 (4), 441–451.

Sophocleous, M., 2002. Interactions between groundwater and surface water: the state of the science. Hydrogeology Journal 10 (1), 52–67.

Sophocleous, M., Perkins, S.P., 2000. Methodology and application of combined watershed and ground-water models in Kansas. Journal of Hydrology 236, 185–201.

Sophocleous, M.A., Koelliker, J.K., Govindaraju, R.S., Birdie, T., Ramireddygari, S.R., Perkins, S.P., 1999. Integrated numerical modelling for basin-wide water management: the case of the Rattlesnake Creek basin in south-central Kansas. Journal of Hydrology 1999, 179–196.

Srivastava, K., Serrano, S.E., Workman, S.R., 2006. Stochastic modelling of transient stream–aquifer interaction with the nonlinear Boussinesq equation. Journal of Hydrology 328, 538–547.

Swain, E.D., Wexler, E.J., 1996. A coupled surface-water and ground-water flow model for simulation of stream-aquifer interaction. US Geological Survey Techniques of Water-Resources Investigations, Book 6, 125 pp, Chapter A6.

Szilagyi, J., Parlange, M.B., Balint, G., 2005. Assessing stream–aquifer interactions through inverse modelling of flow routing. Journal of Hydrology 327, 208–218.

Theis, C.V., 1947. The effect of a well on the flow of a nearby stream. Transactions of the American Geophysical Union 22 (3), 734–738.

USACE, 2002. HEC-RAS, River Analysis System. US Army Corps of Engineers. Hydrologic Engineering Center, v3.1, Nov 2002, CPD-68.

Werner, A.D., Gallagher, M.R., Weeks, S.W., 2006. Regional-scale, fully coupled modelling stream–aquifer interaction in a tropical catchment. Journal of Hydrology 328, 497–510.

Woolhiser, D.A., Liggett, J.A., 1967. Unsteady, one-dimensional flow over a plane — the rising hydrograph. Water Resources Research 3 (3), 753–771.